Design and applications of a scanning SQUID microscope

by J. R. Kirtley
M. B. Ketchen
C. C. Tsuei
J. Z. Sun
W. J. Gallagher
Lock See Yu-Jahnes
A. Gupta

K. G. Stawiasz S. J. Wind

The scanning SQUID (Superconducting Quantum Interference Device) microscope is an extremely sensitive instrument for imaging local magnetic fields. We describe one such instrument which combines a novel pivoting lever mechanism for coarse-scale imaging with a piezoelectric tube scanner for fine-scale scans. The magnetic field sensor is an integrated miniature SQUID magnetometer. This instrument has a demonstrated magnetic field sensitivity of $<10^{-6}$ gauss/ $\sqrt{\text{Hz}}$ at a spatial resolution of \sim 10 μ m. The design and operation of this scanning SQUID microscope are described, and several illustrations of the capabilities of this technique are presented. The absolute calibration of this instrument with an ideal point source, a single vortex trapped in a superconducting film, is shown. The use of this instrument for the first observation of half-integer flux quanta, in tricrystal thin-film rings of YBa₂Cu₃O₇₋₈, is described. The half-integer flux quantum effect is a general test of the symmetry of the superconducting order parameter. One such test rules out symmetry-independent mechanisms for the half-integer flux quantum

effect, and proves that the order parameter in $YBa_2Cu_3O_{7-\delta}$ has lobes and nodes consistent with d-wave symmetry.

Introduction

The Superconducting Quantum Interference Device [1] is the most sensitive magnetic field sensing element known. One version of the SQUID, the thin-film dc SQUID, has two Josephson weak links interrupting a superconducting loop. The maximum supercurrent that can be passed through such a loop before a voltage develops (the critical current) is periodic in the magnetic flux passing through the loop, with period $\Phi_0 = h/2e = 20.7$ gauss- μ m². Typically SQUID electronics dc-bias the device close to the superconducting critical current, apply an ac modulation bias field to the loop, and feed back on a dc bias field to keep the voltage output at the modulation frequency constant. The dc feedback field is then directly proportional to the magnetic flux through the loop. A scanning SQUID microscope scans the SQUID relative to a sample to image the local magnetic fields with unprecedented sensitivity. However, the design of such an instrument provides serious challenges. The SQUID sensor requires a cryogenic environment, since it must be superconducting to operate. The desired scan area, at least

^eCopyright 1995 by International Business Machines Corporation. Copying in printed form for private use is permitted without payment of royalty provided that (1) each reproduction is done without alteration and (2) the *Journal* reference and IBM copyright notice are included on the first page. The title and abstract, but no other portions, of this paper may be copied or distributed royalty free without further permission by computer-based and other information-service systems. Permission to *republish* any other portion of this paper must be obtained from the Editor.

0018-8646/95/\$3.00 © 1995 IBM

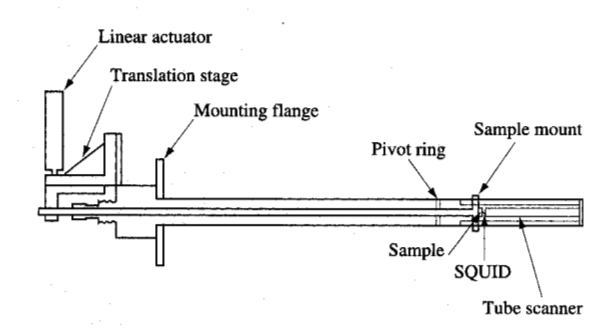


Figure 1
Schematic diagram of our scanning SQUID microscope [16].

a few hundred microns on a side, is extremely difficult to attain at low temperatures using piezoelectric scanning elements. To obtain optimal resolution, it is necessary to make the pickup loop of the SQUID very small, well shielded, and positioned as close as possible to the sample surface. In this paper we describe one such design which meets these difficult requirements.

There are many other techniques for imaging magnetic fields at surfaces [1]: decoration techniques [2], magnetooptical imaging [3], magnetic force microscopy [4], scanning Hall probe microscopy [5], scanning electron microscopy with polarization analysis (SEMPA) [6], and electron holography [7]. Each of these techniques has its own advantages: For example, the magneto-optical techniques are relatively simple and provide the possibility for time-resolved studies, and the electron microscope techniques have very good spatial resolution. The advantage of the scanning SQUID microscope is its very high sensitivity. A comparison of relative sensitivity and resolution for the different techniques appears in [8]. Roughly speaking, the scanning SQUID microscope is orders of magnitude more sensitive to magnetic fields than the other techniques. In addition, it gives an easily calibrated absolute value for the local magnetic fields. Both of these properties are indispensable, for example, for the measurements of the half-integer flux quantum effect described below. A disadvantage of this technique is its relatively poor spatial resolution: Resolution of 10 μ m has been demonstrated, and ultimate resolutions of $<1 \mu m$ seem feasible, but SEMPA [6], for example, has a spatial resolution of 30-50 nm. Nevertheless, there are many possible applications for this technique which do not require submicron spatial resolution.

The first reported scanning SQUID microscope [9] used two sets of orthogonal screw mechanisms operating in liquid helium, driven by room-temperature stepper motors through connecting rods. A commercial radio-frequency (rf) SQUID sensor was inductively coupled to a multi-turn 230- μ m-inside-diameter pickup loop. The spacing between the pickup loop and the sample was fixed by the design of the instrument at about 50 μ m. This microscope was able to detect the presence of single flux quanta trapped in a superconducting niobium thin film, with a signal-to-noise ratio of about 5 and a spatial resolution of 500 μ m.

Succeeding scanning SQUID microscopes [10–14] used a number of different mechanical scanning mechanisms. Vu et al. [8] held the sample fixed at the end of a cryogenic Dewar cold finger. The sensor was attached to the radiation shields of the Dewar, and scanned by moving the radiation shields relative to the cold finger with a translation stage and stepper motors. Vu et al. [12] pivoted the sensor in direct contact with the sample to keep the sensor sample spacing constant during scanning. Black et al. [13] used a system of mechanical wedges driven by rods from room temperature. Ma et al. [14] scanned a room-temperature sample relative to the sensor immersed in liquid helium in a thin-wall Dewar.

Recent scanning SQUID microscopes have replaced discrete, hand-wound pickup loops with either discrete thin-film loops or pickup loops integrated into the SQUID sensor itself. Some designs have used the SQUID as the pickup element. This can be a drawback because of the influence of the fields generated by the SQUID on the system to be measured [13], or these fields can be used to probe the rf susceptibility of the system [15].

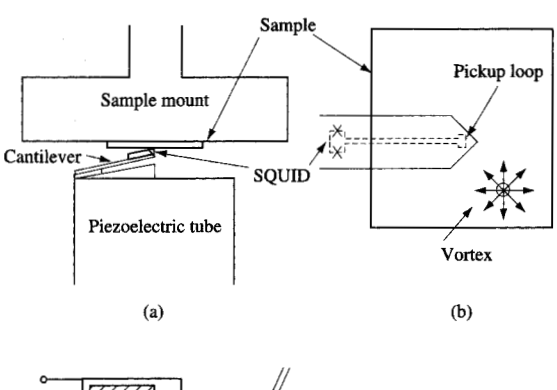
Microscope design

The mechanical scanning mechanism we have designed [16] has the advantage of being extremely simple, while retaining sensitivity and spatial resolution as good as or better than that of the best of the instruments described above. Further, this design should be extendable to an order of magnitude finer resolution than we have demonstrated to date. A schematic drawing of the instrument is shown in Figure 1. The sample is mounted at the end of a long, thin-walled stainless tube. The tube passes through a slip-fit stainless washer about 10 cm from the sample, through a bellows and vacuum tight seal, and is attached to an optical three-axis translation stage. The longitudinal position of the translation stage is adjusted with a differential micrometer. The transverse axes are scanned with dc motors. Longitudinal motion of the translation stage is transmitted directly to the sample mount. Transverse motion of the translation stage is reduced by a factor of 7 to the sample mount, providing finer-scale scanning and minimizing the effects of external vibrations. The microscope is immersed in liquid helium in a μ -metal-shielded Dewar which is suspended from the ceiling of a screened room with elastic cords. We find no noise components from external vibrations. The total scan

range, limited at present by the inside diameter of the vacuum bellows to about 400 μ m, could be significantly increased. We take data in one scan direction and start the scan about 30 μ m before data acquisition in order to minimize the effects of hysteresis. In addition to mechanical scanning, there is also a piezoelectric tube scanner 7 cm long and 0.3 cm in diameter, which scans areas about 20 μ m on a side at low temperatures. This tube scanner also allows mechanical modulation schemes to minimize the effects of low-frequency noise [17]. All of the data presented in this paper were obtained using the mechanical scanning mechanism.

An expanded view of the sample region of the microscope is shown in Figure 2(a). The SOUID sensor is mounted on a cantilever fabricated from a 13-um-thick brass shim, and is run in direct contact with the sample [Figure 2(b)] to compensate for height variations while scanning [12]. We have tested two different types of magnetometer. The first type is a washer SQUID with a ten-turn input coil, and on a second substrate a micronscale pickup loop and "low"-inductance lead structure. Superconducting wire-bonded leads are used to join the two components. The parasitic pickup area of the leads is not a problem if the magnetic fields far from the pickup loop are small or slowly varying. This design, while comparatively complex, has the advantage of allowing the pickup loop structure to be fabricated with a different process than that of the SQUID. For example, in our experiments, the SQUID was fabricated using a planarized all-refractory technology for superconductors (PARTS) [18] process with optical lithography, while pickup loop structures with features down to 0.25 μ m were fabricated using e-beam lithography.

The second type of sensor we used is a fully integrated magnetometer in which the pickup loop and lead structure form an integral part of the SQUID's self-inductance (~100 pH). For the same SQUID technology and pickup loop dimensions, the integrated design is five to ten times more sensitive than the discrete design. Figure 2(c) shows expanded views of the key regions of our original integrated device. The pickup loop is an octagon 10 μ m across, with 1.2- μ m linewidth. There is a 20- μ m-long section of coplanar lead structure with a transition to a low-inductance strip-line. The octagonal pickup loop has an area of 82 μ m², while the coplanar lead structure has an additional pickup area of $\sim 50 \mu \text{m}^2$. The strip-line configuration, which is approximately 1.2 mm in length, is insensitive to normal fields, but has an orthogonal pickup area of 0.3–0.4 μ m² per μ m of strip-line length. The stripline pickup area has not significantly affected the response of the magnetometer in the present microscope geometry. In future designs the strip-line can be replaced with a totally enclosed "coaxial" structure with zero pickup area. The pickup from the coplanar leads is more problematic,



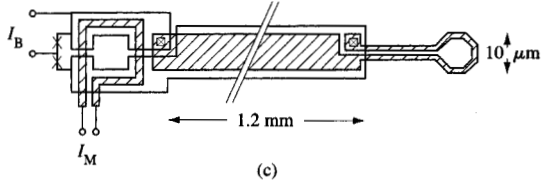


Figure 2

(a, b) Expanded views of the sample area; (c) schematic layout of the integrated magnetometer [16].

but in new designs can be greatly reduced by extending the strip-line structure much closer to the pickup loop. At the other end of the strip-line are the SQUID's junction and modulation structures. The 1-\mu Nb-Al₂O₃-Nb junctions and associated resistive shunts are as described elsewhere [19]. Flux modulation and bias are accomplished by passing current $I_{\rm M}$ through a single-turn coil around a 10-µm-hole-size square washer configured in series with the strip-line and pickup loop. This avoids direct coupling to the measurement volume, which is of concern in designs where the pickup loop constitutes the entire SQUID inductance. The feed of the bias current $I_{\rm R}$ in the present design is asymmetric, a feature that can lead to small shifts in the voltage-flux response along the flux axis as the pickup loop inductance is modulated via proximity to superconducting objects. This effect, while thus far small, can be eliminated by using a resistive split-feed arrangement. Operating in a flux-locked loop at 100 kHz modulation frequency, the noise of the device is typically $<2 \mu \Phi_0/Hz^{1/2}$, corresponding to a field noise at the pickup loop of $\sim 4 \times 10^{-7}$ G/Hz^{1/2}.

The silicon substrate upon which the pickup loop is fabricated is polished to a fine point typically one loop diameter from the center of the pickup loop. An optical image of one such polished tip is shown in **Figure 3**. For most applications the substrate is oriented nearly parallel to the sample plane, with the loop face down and the

Figure 3 Optical image of the tip of a SQUID sensor after polishing.

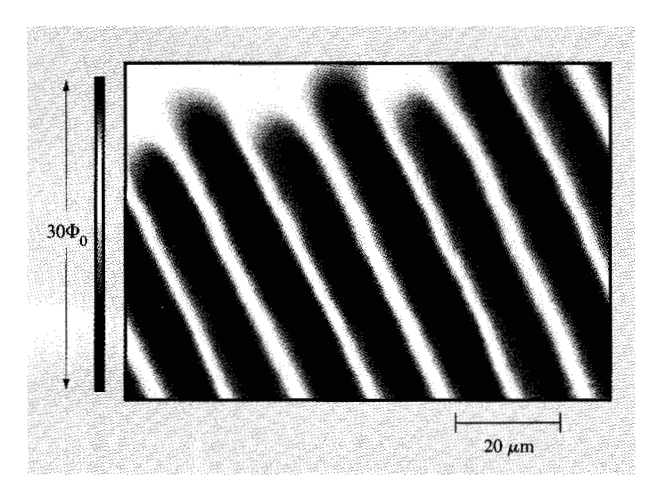


Figure 4

Magnetic image of the alignment track on a 5.25-in. floppy disk. The false-color lookup table scans a range of 30 flux quanta ($\Phi_0 = h/2e$) threading the 10- μ m-diameter pickup loop, oriented normal to the disk surface, with its plane parallel to the bottom of the image.

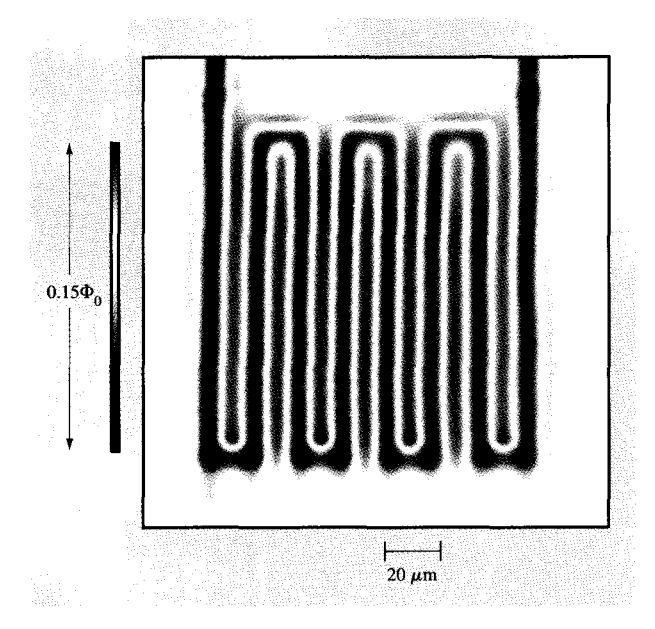
pointed tip in contact with the sample, so that the loop samples primarily the normal component of the field a few microns from the sample surface. The vertical spacing between the loop and the sample, given by the tip-loop distance times the sine of the sample plane/SQUID plane

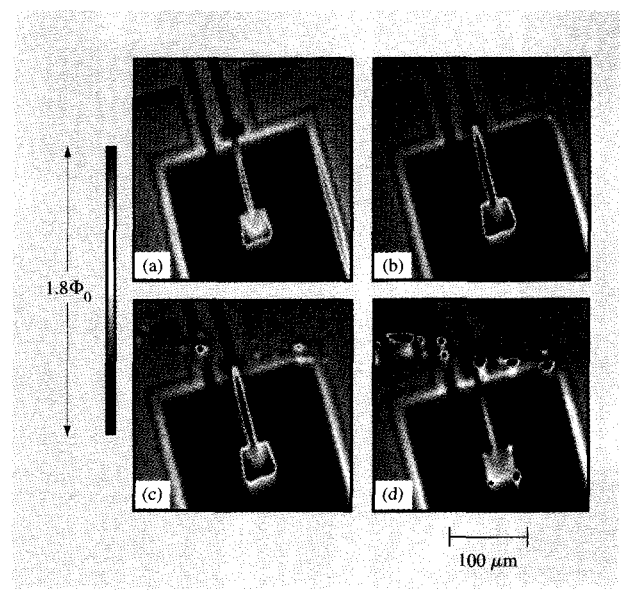
angle, is typically less than the loop diameter, so that resolution and sensitivity are nearly optimized.

Sensitivity

Figure 4 illustrates the sensitivity of the scanning SQUID microscope to permanent magnetic moments. This image is of the magnetic field about 15 μ m above the surface of a commercial 5.25-in.-diameter floppy disk. This particular image was taken with the pickup loop plane oriented normal to the sample and nearly parallel to the track axis (nearly horizontal in this image). The region of the floppy disk that is being imaged contains alignment marks with magnetic domains with moments in the plane of the surface, oriented in alternate directions normal to the track direction. The false-color coding of this image, which appears consistently throughout this paper, uses a spectral distribution from dark blue to bright red. In this image dark blue represents flux passing through the loop in one direction, while red is flux in the opposite direction. The total scale represented by the false-color imaging scheme is about $30\Phi_0$ change in flux through the SQUID pickup loop, corresponding to a total field variation of about 5 gauss. Since the effective noise of the SQUID and electronics, expressed as an effective noise at the SQUID loop, is typically about $2 \times 10^{-6} \Phi_0$, and images are taken at a pixel rate of about 5 Hz, this means that such an image has a potential signal-to-noise ratio of order 10⁷. Other factors, such as the dynamic range of our amplifiers and analog-digital converters, limit the actual signal-to-noise ratio, and there are easier methods for imaging bit patterns, but this is clearly a very sensitive technique. Our calculations indicate that a 1-\mu m-diameter pickup loop spaced 1 μ m from a permanent magnetic source should be able to detect about 100 $\mu_{\rm B}$. The full power of scanning SQUID microscopy will result from applications where this sensitivity is used to advantage.

Figure 5 illustrates the sensitivity of the scanning SQUID microscope to externally applied fields. This is an image of the magnetic field about 2.5 μ m above a thin-film superconducting niobium meander with 10-μm linewidth and spacing. This image was taken with the $10-\mu m$ diameter pickup loop oriented about 20° from parallel to the sample. An external magnetic field of about 5.4 mG was applied to the sample to make the superconducting meander visible. Meissner exclusion of magnetic field from the sample screens the sensor from the applied field above the meander, and concentrates the field in the interline regions. Meissner screening by superconducting thin films is very useful for making index marks for the scanning SQUID microscope using superconducting thin films. The index marks can be made visible by applying a small external field, and made nearly invisible by turning the field off. The "ghosting" visible in the bottom of this image is caused by additional pickup from the unshielded





Magnetic image of the normal component of the field above a superconducting niobium thin-film meander, in the presence of an externally applied 5.3-mG field.

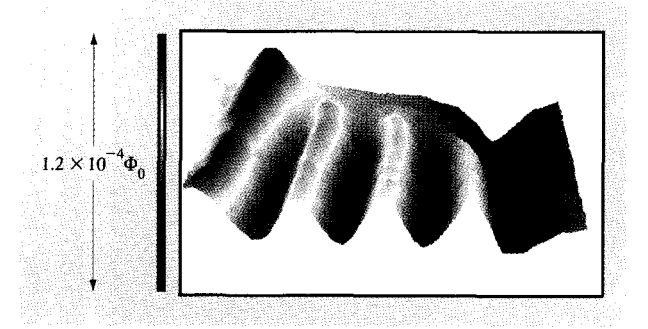


Figure 6

Magnetic image of the field component parallel to the bottom of the image, due to 100-nA ac current through the superconducting niobium meander imaged in Figure 5. This image includes just the top third of the meander.

pickup leads. The influence of the pickup geometry on the observed images is discussed in more detail below.

Figure 6 illustrates the sensitivity of the scanning SQUID microscope to electrical currents. This image is of the upper third of the same niobium thin-film meander as in Figure 5. In this case the 10- μ m-diameter SQUID pickup loop is oriented perpendicular to the sample plane, and nearly parallel to the long lines in the meander pattern.

Figure 7

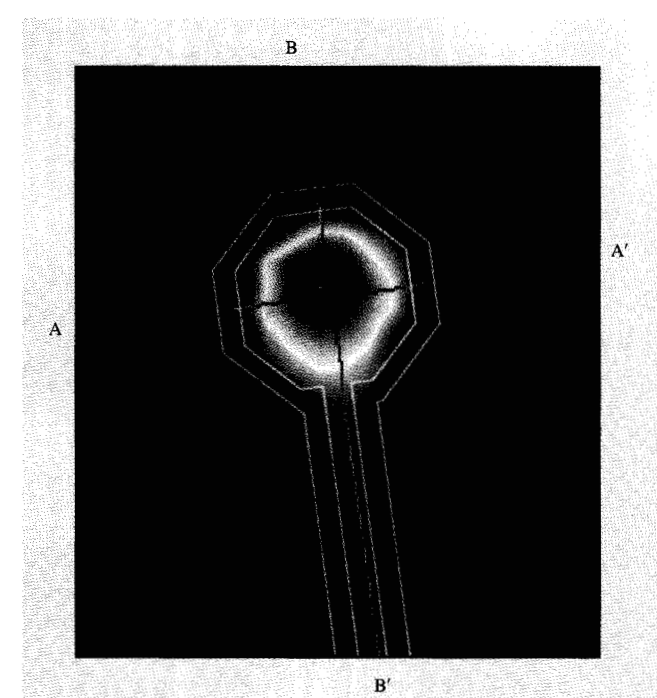
Magnetic image of the normal component of the field above a high- $T_{\rm c}$ YBa₂Cu₃O_{7- δ} thin-film edge-junction washer SQUID, with a scratch running from the upper left to the middle right of the image, first (a) cooled in low field, then (b) cycled to 0.6 G, and (c) to 2.2 G at 4.2 K, and finally (d) cycled to 2.4 G at 77 K. Flux traps first along the scratch, and then at inside corners of the SQUID.

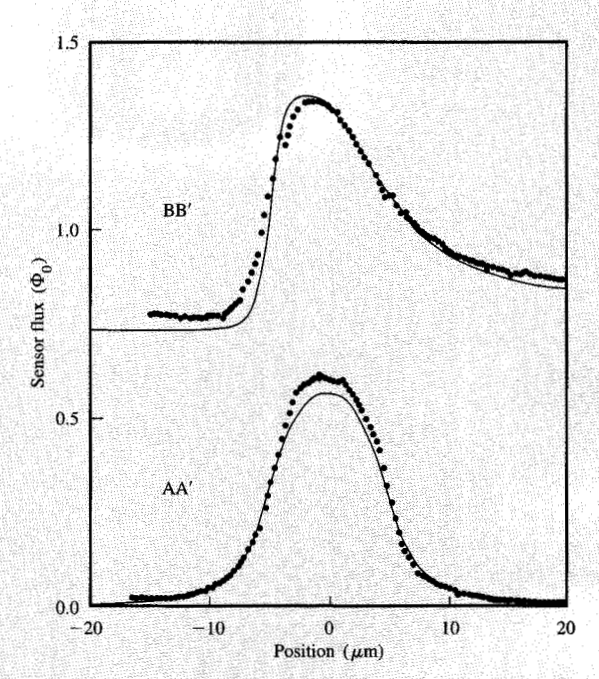
A 134-Hz, 100-nA ac current is applied to the meander. The signal from the SQUID is phase-sensitively detected using a lock-in amplifier. The image shows alternating magnetic field directions associated with the alternating current directions as the current follows the meander pattern. The point-to-point rms noise in this image corresponds to an effective noise at the SQUID loop of $2.5 \times 10^{-6} \Phi_0$, corresponding to an effective current noise of about 1 nA/ $\sqrt{\rm Hz}$.

Applications

• Imaging of superconducting circuitry

As an example of an application of this technique, the images in Figure 7 show the normal component of the magnetic field above a high- $T_{\rm c}$ thin-film YBa₂Cu₃O_{7- δ} step-edge-junction washer SQUID [20], imaged using the integrated SQUID magnetometer. It is desirable for device applications to minimize hysteresis in the SQUID response vs. applied field characteristics. Such hysteresis can result from trapping and motion of vortices in the superconducting film [21]. The device imaged in Figure 7, which has a scratch running through it from the upper left to center right of the image, has particularly large hysteresis. All of the images in Figure 7 were taken at





Expanded view of the magnetic image of an individual flux vortex in $YBa_2Cu_3O_{7-8}$, with the actual pickup loop geometry superposed. The diameter of the pickup loop is $10 \mu m$, with $1.2-\mu m$ linewidths. The dots in the right portion of the figure are cross sections through the data as indicated by the contrasting lines. The solid lines are fits to the data assuming a vortex with h/2e flux, numerically integrating over the known pickup loop geometry, with the distance between the tip contact point and the center of the pickup loop as the only fitting parameter [16].

4.2 K in an applied field less than 2 mG. Figure 7(a) images the sample as cooled in a field of about 2 mG. Eighteen trapped bulk vortices are visible in the dark green "washer" of this device. This trapped flux generates screening currents which circulate around the device, generating fields which make the outline of the device visible, even in the absence of an external applied field. The image of Figure 7(b) was taken after the device was cycled to 0.6 G at 4.2 K. Notice that a single flux "bundle" is trapped in the upper right corner of the device washer, just where the scratch crosses it. Figure 7(c) was taken after the device was cycled to 2.2 G at 4.2 K. As the sample was cycled to successively higher fields, more flux was trapped along the scratch. Finally, the image in Figure 7(d) was taken after the sample was cycled to 2.4 G at 77 K before cooling to 4.2 K for imaging. In addition to flux trapped in the scratch, vortices are also trapped in the inside corners of the square hole in the washer. These images show that flux traps first at thin-film defects, and then at locations where the magnetic field strengths are largest—at inside corners.

Figure 8 shows an expanded view of one of the flux vortices trapped in the bulk of the SQUID washer of

Figure 7. Superposed on the magnetic image is a scaled and properly oriented schematic of the sensor SQUID pickup loop and leads. This superposition shows that the shape of the vortex image is determined by the shape of the pickup loop, the asymmetry being a direct consequence of the pickup area of the coplanar leads. The field from an isolated superconducting vortex is given by

$$\hat{B}(\hat{r}) = \frac{\Phi_0}{2\pi r^3} \hat{r} \tag{1}$$

for distances r much greater than the penetration depth. The sensitivity of this instrument can be estimated by considering a circular loop of radius r_0 parallel to a superconducting surface and centered a height h above a flux vortex trapped in the superconductor. The total flux through this loop is

$$\Phi_{\text{loop}} = \Phi_0 \left[1 - \frac{h/r_0}{\sqrt{(h/r_0)^2 + 1}} \right]. \tag{2}$$

At the easily attained height $h = r_0$, the amount of flux coupling into the pickup loop is about $0.3\Phi_0$. Typically our

660

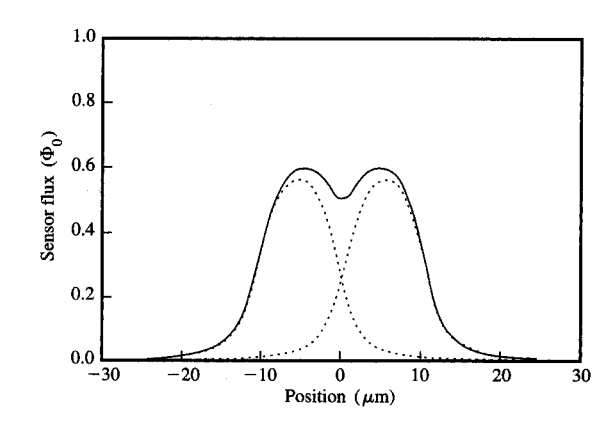
images are taken at about 5 pixels/s, which means that with a SQUID noise of $2 \times 10^{-6} \Phi_0/Hz^{1/2}$ an individual vortex can be imaged with an electronic signal-to-noise ratio of about 7×10^4 . Actual signal-to-noise ratios, although limited by scanning irregularities apparently arising from tip-sample interactions, are nevertheless remarkably good, as can be seen from the cross sections in Figure 8. The solid lines in Figure 8 are fits to the data numerically integrating Equation (1), using the known pickup loop and lead geometry, the known angle of the SQUID plane relative to the sample plane ($\sim 20^{\circ}$), with the distance between the tip and the pickup loop center as the only fitting parameter. The best fit was obtained for a distance of 8 µm, in reasonable agreement with microscopic inspection of the tip after polishing. The fits show that we have a good understanding of the absolute magnitude and general shape of the observed vortex images.

The resolution of the instrument can be defined using a Rayleigh-like criterion [22], as illustrated in **Figure 9**. This figure shows the cross sections predicted for the loop geometry and orientation of Figure 8, for two point vortices. The dashed lines are the individual contributions, and the solid line is the total predicted signal. The spacing between the two vortices has been adjusted until the predicted minimum is 81% of the maxima. This happens for a spacing of 11.2 μ m. We therefore define the resolution of this tip-loop geometry and orientation as 11.2 μ m.

Figure 10 shows the predicted resolution and total flux coupling into the loop for magnetic monopole sources, such as superconducting vortices, using the Rayleigh-like criterion, assuming a hexagonal pickup loop oriented parallel to the sample surface. This figure shows that the ultimate resolution is set by the diameter of the loop, and that the signal falls off rapidly as the loop is moved away from the surface. These curves would look different, for example, for a dipole source, but superconducting vortices provide a convenient calibration point source for the scanning SQUID microscope.

• Half-integer flux quantum effect

Perhaps the single most contested issue in solid-state physics at present is the mechanism for superconductivity in the high-critical-temperature copper—oxide ceramic superconductors. An unambiguous determination of the order parameter symmetry is crucial to understanding this mechanism. For example, spin-mediated coupling mechanisms can be nearly ruled out if the order parameter does not have $d_{x^2-y^2}$ symmetry $[\Delta(\hat{k}) \sim k_x^2 - k_y^2 \sim \cos 2\theta]$ [23]. Recently, there have been numerous experiments [24–29] dealing with various aspects of pairing symmetry in high- T_c superconductors. A number of experimental tests which favor d-wave symmetry are sensitive only to



Finance 9

Predicted SQUID output signal for two superconducting vortices separated by 11.2 μ m, assuming a 10- μ m-diameter pickup loop with the geometry shown in Figure 8. The dashed lines are the contributions from the two individual vortices; the solid line is the total predicted signal. The spacing has been adjusted so that the minimum between the two vortex positions is 81% of the maximum amplitude. We define the resolution of this geometry to be 11.2 μ m, following a Rayleigh-like criterion.

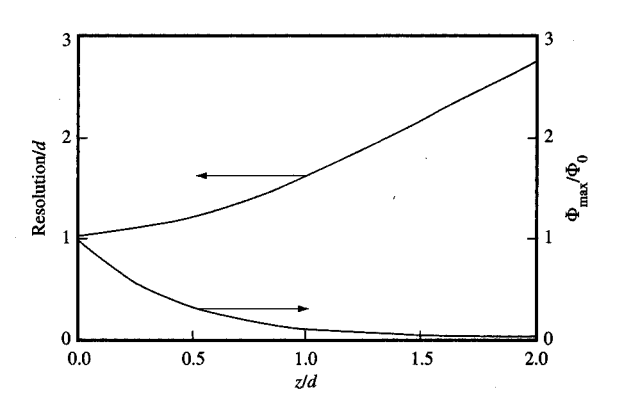
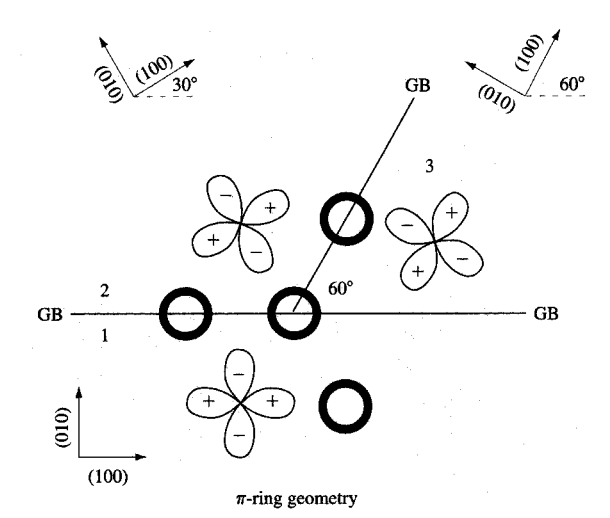


Figure 10

Predicted resolution (upper curve) and maximum flux coupled (lower curve) for a hexagonal loop of diameter d, as a function of the reduced height z above the sample plane, using a Rayleigh-like criterion outlined in Figure 9.

the absolute number of states in the gap, often only in the surface of the sample. A more unambiguous test of d-wave symmetry would be one that is sensitive to the sign of the order parameter. One such test was proposed several years ago [30] and performed by Wollman et al. [25]. This test measures the critical current of a SQUID fabricated with a



Schematic diagram of the tricrystal $YBa_2Cu_3O_{7-\delta}$ ring samples used to observe the half-integer flux quantum effect. Three c-axisup crystals of SrTiO3 with the indicated orientations are polished and fused so that they meet at a single tricrystal point. YBa₂Cu₃O_{7-δ} grown epitaxially on the tricrystal substrate forms grain-boundary (GB) weak-link Josephson junctions where the substrates meet. The YBa₂Cu₃O₇₋₈ is photolithographically defined and ion-etched to form four rings, one with no junctions, two with two junctions, and one with three junctions. Superposed on the diagram are polar plots of the angular dependence of a gap with assumed d-wave functional form, oriented along the crystalline axes. In this geometry there is an odd number of sign changes of the normal component of the superconducting order parameter for the three-junction ring, if YBa₂Cu₃O₇₋₈ is a d-wave superconductor. This sign change is predicted to cause a spontaneous magnetization of a half-flux quantum in the threejunction ring, which is in fact observed.

superconducting Pb film forming Josephson junctions with two adjacent corners of a YBa $_2$ Cu $_3$ O $_{7-\delta}$ single crystal. If YBa $_2$ Cu $_3$ O $_{7-\delta}$ were an s-wave superconductor, such a SQUID would be expected to show the conventional maximum critical current at zero applied field. A d-wave superconductor, on the other hand, should experience canceling contributions from supercurrents of opposite signs on the two orthogonal faces, and should have a minimum supercurrent at zero applied bias. The latter effect was in fact observed, supporting d-wave symmetry for YBa $_2$ Cu $_3$ O $_{7-\delta}$. However, this experiment was subject to a great deal of criticism, because of possible interferences introduced by trapped flux, flux focusing effects at corners, and difficulties in extrapolating the experimental data to zero voltage.

Recently Tsuei et al. [31] proposed a definitive test of the symmetry of the YBa₂Cu₃O_{7- δ} order parameter that

depends on the principle of flux quantization, rather than on details of the SQUID current-voltage characteristic, and used the scanning SQUID microscope described in this paper to make this test. The basic idea behind this test is as follows: Consider a superconducting ring that is interrupted by one Josephson weak link with a change in sign of the order parameter across the weak link boundary. This discontinuity costs Josephson coupling energy. If this Josephson coupling energy is sufficiently large to overcome the inductive energy associated with supercurrent around the ring, it is energetically favorable for the ring to spontaneously generate sufficient supercurrent to have exactly half of the conventional flux quantum, $\Phi_0/2 = h/4e$, threading the ring. It is very difficult to design a ring with a sign change across just one junction, but the same physics holds for rings with an odd number of sign changes. Tsuei et al. proposed a three-junction tricrystal geometry that should show the half-integer spontaneous magnetization if the superconducting order parameter in YBa, $Cu_3O_{7-\delta}$ has d-wave symmetry.

Figure 11 shows a schematic of the sample used by Tsuei et al. [31] to make the first measurements of the halfinteger flux quantum. The sample is fabricated on a SrTiO₃ substrate that was cut into three pieces, reoriented, polished, and fused to form a tricrystal substrate with the crystalline orientations indicated in Figure 11. YBa, Cu, O₇₋₈ was epitaxially grown with the c-axis up on the tricrystal substrate, forming grain boundaries (GB) at the boundaries between the sections of the underlying substrate. These boundaries act as Josephson weak links between the sections of the thin-film weak links. As pointed out by Sigrist and Rice [32], since the Josephson critical current across such a weak link is dominated by tunneling from Cooper pairs propagating normal to the interface, this critical current is proportional to the product of the projections onto the interface normal of the momentum-dependent order parameters on the two sides of the interface. This is indicated schematically for an assumed d-wave symmetry of the order parameter in Figure 11. The polar plots in this figure indicate the magnitude of the order parameter $(k_r^2 - k_v^2)$ as a function of Cooper pair momentum in the crystal coordinate system. These polar plots show that one of the interfaces, between sections 1 and 3 of the central three-junction ring, has a negative Josephson critical current. The Josephson relation between the current I and the order parameter phase difference ϕ across the junction can then be written as

$$I = -|I_c|\sin(\phi) = |I_c|\sin(\phi + \pi), \tag{3}$$

where $I_{\rm c}$ is the critical current of the junction. A junction with a negative critical current is called a π -junction; a ring with an odd number of π -junctions is called a π -ring. Signist and Rice [32] showed that a single-junction π -ring

should have half-integer spontaneous magnetization. Tsuei et al. [31] extended this analysis to show that π -rings with multiple junctions should also show this effect. Tsuei et al. [31] also showed that the geometry indicated schematically in Figure 11 should exhibit the half-integer effect independent of the degree of interface roughness present.

There is an intrinsic degeneracy involved in this analysis: The positive lobe of the polar plots in Figure 11 can be arbitrarily assigned to either the (100) or (010) directions in any of the three regions. It is easy to show that however these assignments are made, the three-junction ring always has either one or three negative critical currents, so that the half-integer flux quantum effect should always be observed. The $YBa_2Cu_3O_{7-\delta}$ films grown in this way are highly twinned. However, twin boundaries are very strong Josephson links, so that the order parameter in one particular section of a ring should be tightly coupled, with discontinuous changes in the phase only occurring at the grain boundaries.

In this experiment, four rings (inner diameter = 48 μ m, width = 10 μ m) are patterned using a standard photolithographic process. To test the quality of the individual grain-boundary junctions across each grain boundary, bridges 25 μ m in length and 10 μ m in width across each grain boundary are prepared on bicrystal substrates that were cut off from the tricrystal substrate. The epitaxial YBa₂Cu₃O₇₋₈ films for these junctions were laser-deposited in the same run and in close proximity to the tricrystal substrate for the four rings. The values of I_a^{η} (J_c^{η}) for these three test junctions agree within 20%. I_c^{ij} (J_c^{ij}) is found to be 1.8 mA (1.5 × 10⁵ A/cm²). The resistive transitions of these films were sharp, with a small shoulder below the T_c (= 90.7 K) characteristic of a grain-boundary weak link. The IV curve of the control junctions exhibited a typical RSJ Josephson junction characteristic.

From the $I_{\rm c}^{ij}$ value and the estimated self-inductance of the rings ($L \approx 100~{\rm pH}$) one finds that the $LI_{\rm c}^{ij}$ product is about $100\Phi_0$, easily satisfying the condition $LI_{\rm c}^{ij} \gg \Phi_0$ required by the energy considerations described above. Therefore, a spontaneous magnetization of $\Phi_0/2$ at $\Phi_{\rm ext} \sim 0$ should be observable in our three-junction ring.

Figure 12 shows a scanning SQUID microscope image of the four rings of Figure 11. This image was obtained at 4.2 K with a 10- μ m-diameter pickup loop rotated approximately 20° away from parallel to the sample plane. The ratio of the mutual inductance between loop and ring to the self-inductance of the ring is about 0.02, so that the effect of the SQUID flux coupling back into the ring should be small. Our interpretation of this image is that the outer zero-junction ring (lower left in this image) and two-junction rings (right and upper left) have no flux threading them, while the central three-junction ring has half of the

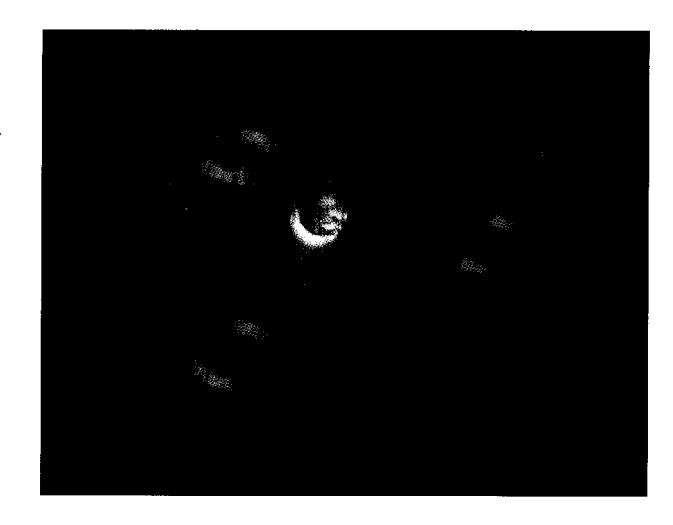


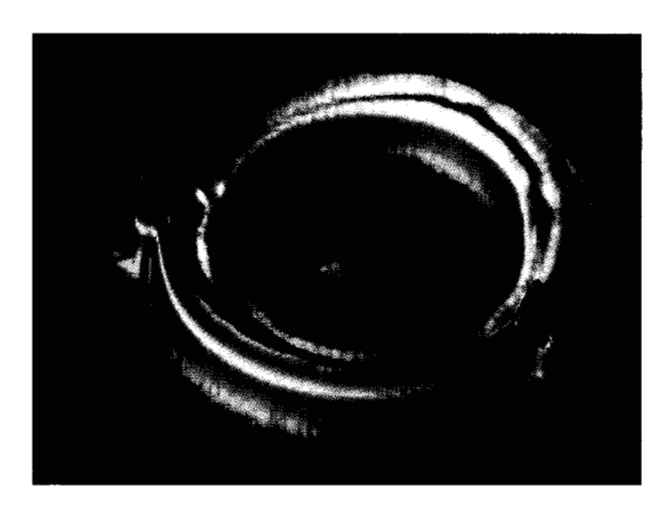
Figure 12

Magnetic image of the tricrystal YBa₂Cu₃O_{7- δ} ring sample of Figure 11. The outer zero- and two-junction rings have no flux trapped in them; the center three-junction ring has $\Phi_0/2 = h/4e$ flux trapped in it. The outer rings are visible because of slight changes in the inductance of the sensor SQUID when it is directly above the edge of a superconducting ring [36].

flux quantum h/2e threading it. The outer control rings are visible through mutual inductance coupling between the rings and the SQUID loop.

The image of the half-flux quantum in the central ring of Figure 12 is asymmetric because of the additional pickup area of the unshielded leads in this sensor geometry. We have recently repeated these measurements with a loop with a 4- μ m pickup loop diameter, with much better shielding of the leads. These images show much less asymmetry, as well as much better spatial resolution. Since the circulating supercurrents associated with the half-flux quantum are localized in a nearly twodimensional plane, it is possible to deconvolute the magnetic field images to obtain the current distribution [33]. Figure 13 shows a deconvoluted image of the circulating supercurrents associated with the half-flux quantum in the ground state of the three-junction ring. There are two spikes in the data which are associated with flaws in the edges of the ring. This image shows that the supercurrents are in fact slightly localized at the edges of the ring due to self-screening effects. There is about 10 μA of supercurrent flowing around the ring in this image.

It is extremely important to determine exactly how much flux is trapped in the rings. We determined the amount of flux in each ring using three different methods, which agree with one another to within 10%. The first method is direct calculation. The mutual inductance $M(\rho)$ between a pickup loop tilted at an angle θ from the sample



Deconvoluted image of the supercurrent in the three-junction ring when it has a half-flux quantum trapped in it. The two peaks are artifacts from defects at the edges of the ring. This image was taken with a $4-\mu$ m-diameter pickup loop SQUID sensor.

(xy) plane in the xz plane, and a circular wire of radius R at the origin, is given by

$$M(\rho) = \frac{\mu_0 R}{4\pi} \int d^2x \int_0^{2\pi} d\phi$$

$$\times \frac{\{\cos\theta (R - y \sin\phi - x \cos\phi) - \sin\theta (z \cos\phi)\}}{(x^2 + y^2 + z^2 + R^2 - 2xR \cos\phi - 2yR \sin\phi)^{3/2}},$$
(4)

where the integral d^2x is over the plane of the pickup loop, and the vector ρ specifies the displacement of the pickup loop with respect to the ring in the xy plane. We calculate M(0)=2.4 pH for the as-fabricated tip centered above a 29- μ m-radius ring, at a tilt angle of 20° . A given flux Φ threading a superconducting ring with self-inductance L induces a circulating current $I_r = \Phi/L$ around the ring, which in turn induces a flux $\Phi_s(\rho) = M(\rho)\Phi/L$ in the pickup (sensor) loop. We calculate the inductance of our rings to be 99 ± 5 pH.

Figure 14 shows a top view of the same data as in Figure 12. The solid lines in the bottom part of Figure 14 are model calculations for the cross sections indicated by the contrasting lines in the image, assuming that $\Phi = \Phi_0/2 = h/4e$ in the three-junction ring. The asymmetry in the images results from the tilt of the pickup loop, as well as the asymmetric pickup area from the unshielded section of the leads. Clearly, using $\Phi_0/2$ for the flux in the three-junction ring results in much better agreement than would be obtained using Φ_0 .

The second method for calibrating the response of the SQUID pickup loop to flux in the rings is made by

positioning the pickup loop in the centers of the rings and measuring the SOUID output vs. field characteristic. Representative results for the three-junction ring are shown in Figure 15(a). In this figure a linear background, measured by placing the loop over the center of the zerojunction control ring, has been subtracted out. The upper insert in this figure shows the sensor flux vs. field characteristic over a larger field range. At low fields, stepwise admission of flux into the ring leads to a staircase pattern, with progressively smaller heights and widths to the steps, until over a small intermediate field range, shown for increasing field in the main part of Figure 15(a), single flux quanta are admitted. We interpret the "noise" in these data as flux motion in the grain boundaries and the other rings. At larger fields the steps disappear and the SQUID flux vs. field characteristic slowly oscillates about a mean line. The heights of the single flux-quantum steps in the intermediate field region, derived by fitting the data to a linear staircase (dashed line) are $\Delta \Phi_s = 0.0237 \Phi_0$. This is in good agreement with our calculated value of $\Delta\Phi_s$ = $M(0)\Phi_0/L = 0.024 \pm 0.003\Phi_0$. Twelve repetitions of this measurement, including measurements of both the twojunction and three-junction rings, gave values of $M(0)\Phi_0/L$ = $0.028 \pm 0.005\Phi_0$. The large uncertainties in these calibration runs have two sources: Small misalignments in the position of the loop relative to the center of the rings result in relatively large errors, as can be seen from the cross sections of Figure 14. Further, the step heights on average increase with time, as the tip wears while taking =100 images in direct contact with the sample, moving the pickup loop progressively closer to the ring plane. Visual inspection of the loop at the end of these measurements showed extensive wear, such that the point of contact was within 2 μ m of the pickup loop edge.

We calibrated our fields by replacing the sample with a large-pickup-area SQUID magnetometer. Our measured fields agree with our calculations to within about 3%. The widths of the steps, averaging 11 measurements for increasing positive fields, were 5.7 \pm 1 mG. This is about 25% smaller than $\Delta B = \Phi_0/A_{\rm ring}$, where $A_{\rm ring} = 2642~\mu {\rm m}^2$ is the effective area of the rings. This is not too surprising, given the nonequilibrium nature of the flux penetration process, as indicated by the hysteresis in the flux-field characteristic. The average slope of the flux-field characteristic does, however, agree within experimental error with the effective area of the rings.

Figure 15(b) summarizes the results from twelve cooldowns of the sample. We plot the absolute value of the difference between the SQUID loop flux in the centers of the two-junction or three-junction rings, and the zero-junction control ring. Since each point was taken from a full image, we could judge the center of the rings with accuracy, and our data scatter is much smaller than in the

calibration runs. The solid lines are the expected values for the flux difference, calculated as described above. In all of our measurements $\Delta\Phi$ always fell close to (N+1/2) (h/2e) for the three-junction ring, and close to Nh/2e for the two-junction rings (N) is an integer). However, there is clearly some drift to the data, which we associate with tip wear. A fit to the eight $\Phi_0/2$ points in Figure 15(b), assuming that exactly h/4e flux threads the three-junction rings, implies that the mutual inductance M(0) is 2.4 pH for the as-fabricated tip and increases to 2.9 pH at the end of the series. For comparison, our calculations give 2.4 pH for the center of the loop 10 μ m from the tip end, and 2.7 pH for the tip end just at the edge of the pickup loop. The dashed lines, including this correction to the mutual inductance, agree remarkably well with the data.

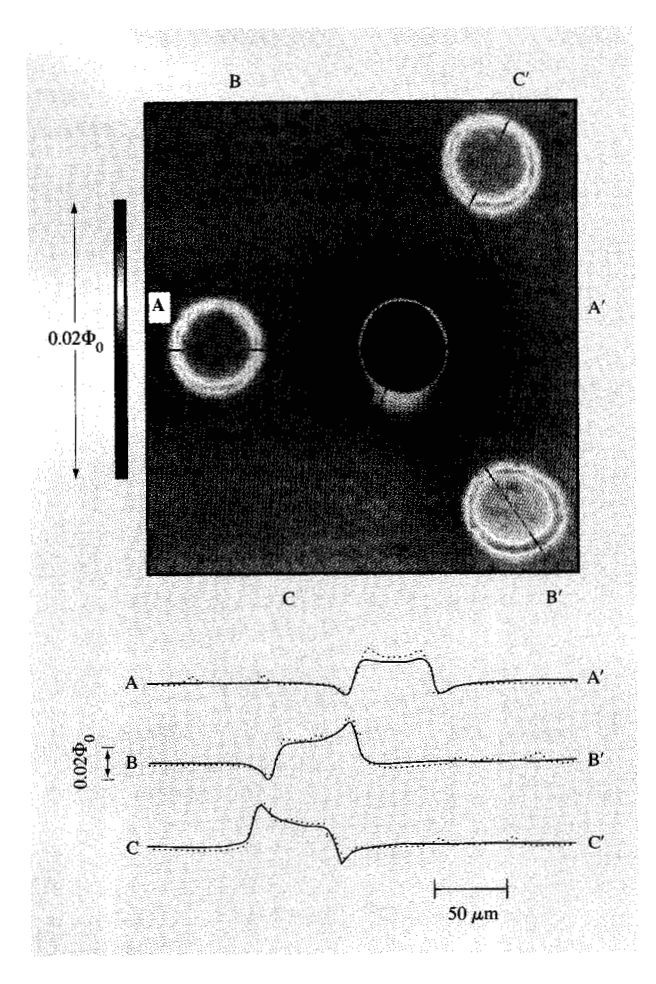
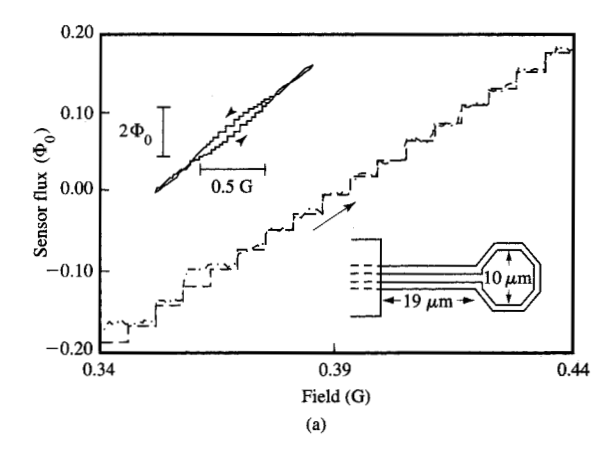
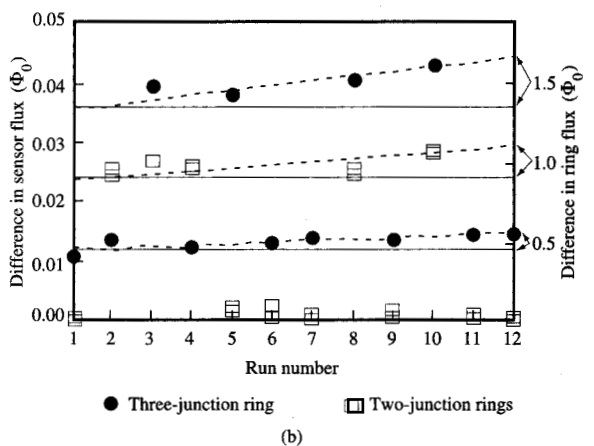


Figure 14

Top-view magnetic field image of the sample of Figure 11, cooled in a field <5 mG. The dots are cross sections through the data, as indicated by the contrasting lines. The solid lines are calculations assuming the three-junction ring has $\Phi_0/2$ flux threading it [31].

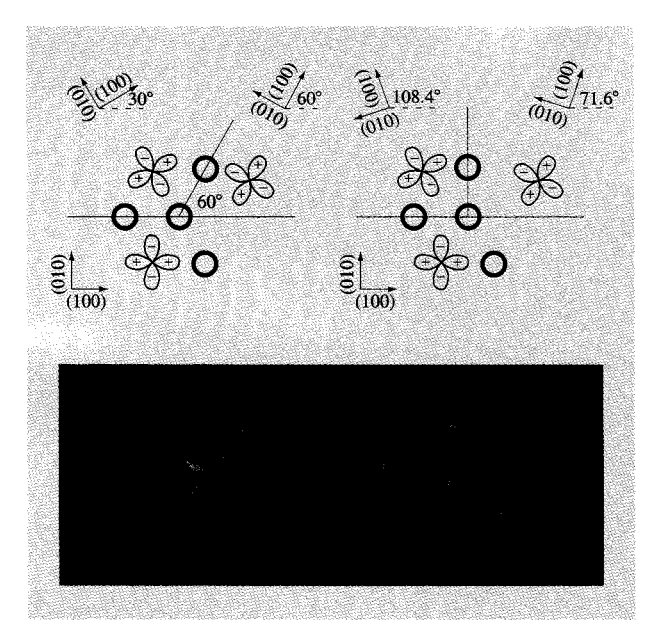




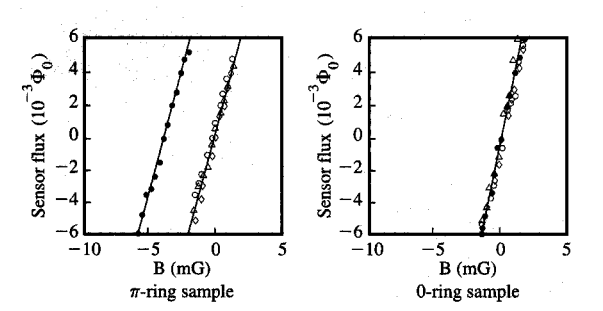
Eldura 15

(a) Measured SQUID flux vs. field characteristic with the SQUID pickup coil centered on the three-junction ring. The upper left insert shows the flux-field characteristic over a larger field range. The lower right insert shows the geometry of the SQUID pickup loop, with 1.2-\(\mu\mathbb{m}\mathbb{m}\) line widths and spacings. (b) Result of 12 separate cooldowns of the sample in nominal zero field. The solid lines are our calculations for the as-fabricated tip; the dashed lines include a correction for tip wear [31].

These experiments show clearly that the three-junction ring spontaneously magnetizes with half of the conventional flux quantum in it, consistent with the order parameter in YBa₂Cu₃O_{7- δ} having d-wave symmetry. However, there have been at least two alternate mechanisms, spin-flip scattering by magnetic impurities at the tunnel barrier [34] and indirect tunneling through a localized state (correlation effects) [35], suggested to cause π -phase shifts at the junction interfaces, resulting in π -rings in our three-junction rings. Kirtley et al. [36] have designed a tricrystal substrate with angles chosen so that, according to the predictions for d-wave pairing, the three-



The upper part of the figure [36] is a schematic of two tricrystal YBa₂Cu₃O₇₋₈ ring samples. The π -ring sample is designed to exhibit the half-integer flux quantum effect if YBa₂Cu₃O₇₋₈ is a d-wave superconductor; the 0-ring sample is designed not to show this effect. The bottom part of the figure compares the scanning SQUID microscope images of these samples, cooled in nominally zero field. Only the π -ring sample shows the half-integer flux quantum effect, proving that the superconducting order parameter in YBa₂Cu₃O₇₋₈ has nodes and lobes consistent with d-wave symmetry.



∘ Zero-junction ∘ Left two-junction △ Top two-junction • Three-junction

Figure 17

Difference in sensor flux for the sensor positioned at the center of the ring vs. outside the ring, for all of the rings, for both sample geometries of Figure 16. Measurement of the zero intercepts of the lines gives a value of $0.505 \pm 0.02\Phi_0$ flux enclosed in the π -ring, while the other rings have $0.0 \pm 0.01\Phi_0$ [36].

junction rings will not be π -rings, either in the clean (smooth interface) or dirty (rough interface) limits. The failure to observe half-integer flux quantization in this geometry would rule out symmetry-independent mechanisms.

Figure 16 shows the actual design parameters for the two samples. Junctions result each time a ring crosses a grain boundary. The zero-junction rings and two-junction rings should show integer flux quantization. Only the three-junction ring in the π -ring geometry should show the half-integer quantum effect if it is due to nodes in the superconducting order parameter, but both three-junction rings should show the effect if it is due to a symmetry-independent mechanism. The only difference between sample fabrication and measurement of the two samples was the tricrystal substrate geometry.

Figure 16 compares scanning SQUID microscope images from a YBa₂Cu₃O₇₋₈ tricrystal ring sample with the π -ring geometry (left) and the 0-ring geometry (right) cooled to the measuring temperature of 4.2 K in fields less than 2 mG. The images were taken with the SQUID substrate oriented about 20° from parallel to and in direct contact with the sample, so that the loop sampled primarily the normal component of the magnetic field about 5 μ m above the sample surface. The flux threading through the center three-junction ring in the π -ring geometry sample (a) is very close to $\Phi_0/2$, while the others have very close to 0 flux. The false-color table in this image spans a range of $0.03\Phi_0$ change in flux through the sensor SQUID. Images taken with these samples cooled in different fields showed that the three-junction π -ring always had $(N + 1/2)\Phi_0$ (N is an integer) flux in it, while the three-junction 0-ring always had $N\Phi_0$, ruling out symmetry-independent mechanisms for the half-integer flux quantization.

The calculation of the intensities of the scanning SQUID ring images described above requires detailed knowledge of the self-inductance of the rings and the mutual inductance between the rings and the pickup loop [31]. Results from a more direct, accurate, and absolute method are presented in Figure 17. This figure shows the SQUID sensor signal at the center of the ring, relative to the signal outside the ring, for all of the rings as a function of field applied by a coil surrounding the microscope. The SQUID difference signal goes to zero when there is as much flux inside the ring as outside it. Therefore, the difference in flux through the rings is just the difference in applied field required to make the signal go to zero times the effective area of the ring. Estimating the effective area of the rings [36] to be $\sim \pi [(r_{in} + r_{out})/2]^2 = 2642 \pm 80 \ \mu \text{m}^2$, where $r_{\rm in}$ = 24 $\mu \rm m$ and $r_{\rm out}$ = 34 $\mu \rm m$ are respectively the inner and outer radii of the rings, the three-junction ring in Figure 15(a) has $0.505 \pm 0.02\Phi_0$ more flux threading through it than the zero-junction or two-junction rings. Further, the difference in flux between any of the other rings in either the π -ring or the 0-ring geometries is $|\Delta\Phi| < 0.01\Phi_0$. Our

calculations indicate that any, e.g., s-wave component to a presumed s + id superconducting order parameter would alter the flux quantization condition away from exactly $\Phi_0/2$ by roughly the fractional portion that is s-wave. These experiments therefore indicate that the superconducting order parameter has lobes and nodes consistent with d-wave symmetry and put experimental limits of about 4% on any out-of-phase s-wave component in YBa₂Cu₃O_{7- δ}.

Conclusion

In conclusion, the scanning SQUID microscope represents a very sensitive instrument for imaging local magnetic fields. Currently, resolution of 10 $\mu \rm m$ has been demonstrated; ultimately an order of magnitude better resolution should be possible. The sensitivity of this instrument is such that spins of about a hundred $\mu_{\rm B}$, or currents of a few nA, can be imaged. This sensitivity allows measurements that would be extremely difficult using any other technique, such as the first observation of the half-integer flux quantum effect.

Acknowledgments

We thank Margaret Manny, Dale Pearson, and the . Yorktown Silicon Facility for help in fabrication of the magnetometer and some of the early SQUID pickup loops. We would also like to thank M. Bhushan for fabrication of the high-resolution sensors mentioned briefly here. The technical assistance of S. H. Blanton, G. Trafas, M. Cali, and J. Hurd is greatly appreciated. Useful discussions with D. J. Scalapino, D. H. Lee, D. M. Newns, M. Sigrist, and P. Chaudhari are gratefully acknowledged. This work was performed under the auspices of the Consortium for Superconducting Electronics, which is partially supported by the Advanced Research Projects Agency under Contract No. MDA972-90-C-0021.

References and notes

- 1. A recent popular review of SQUIDs appears in J. Clarke, Sci. Amer., August 1994, p. 46.
- An excellent recent review of decoration techniques appears in D. J. Bishop, P. L. Gammel, D. A. Huse, and C. A. Murray, Science 255, 165 (1992).
- 3. S. Gotoh and N. Koshizuka, Phys. C 176, 300 (1991).
- D. Rugar, H. J. Mamin, P. Guethner, S. E. Lambert, J. E. Stern, I. McFadyen, and T. Yogi, J. Appl. Phys. 68, 1169 (1990).
- A. M. Chang, H. D. Hallen, L. Harriott, H. F. Hess, H. L. Kao, J. Kwo, R. E. Miller, R. Wolfe, and J. van der Ziel, Appl. Phys. Lett. 61, 1974 (1992).
- M. R. Scheinfein, J. Unguris, M. H. Kelley, D. T. Pierce, and R. J. Celotta, Rev. Sci. Instrum. 61, 2501 (1990).
- K. Harada, T. Matsuda, J. Bonevich, M. Igarashi, S. Kondo, G. Pozzi, U. Kawabe, and A. Tonomura, *Nature* 360, 51 (1992).
- 8. L. N. Vu and D. J. Van Harlingen, *IEEE Trans. Appl. Supercond.* 3, 1918 (1993).
- F. P. Rogers, Master's Thesis, Massachusetts Institute of Technology, Cambridge, MA, 1983.

- H. Minami, Q. Geng, K. Chihara, J. Yuyama, and E. Goto, *Cryogen.* 32, 648 (1992).
- A. Mathai, D. Song, Y. Gim, and F. C. Wellstood, Appl. Phys. Lett. 61, 598 (1993).
- L. N. Vu, M. S. Wistrom, and D. J. Van Harlingen, *Appl. Phys. Lett.* 63, 1693 (1993).
- R. C. Black, A. Mathai, F. C. Wellstood, E. Dantsker, A. H. Miklich, D. T. Nemeth, J. J. Kingston, and J. Clarke, *Appl. Phys. Lett.* 62, 2128 (1993).
- 14. Y. P. Ma, I. M. Thomas, A. Lauder, and J. P. Wikswo, *IEEE Trans. Appl. Supercond.* 3, 1941 (1993).
- R. C. Black, F. C. Wellstood, E. Dantsker, A. H. Miklich, D. T. Nemeth, D. Koelle, F. Ludwig, and J. Clarke, Appl. Phys. Lett. 66, 99 (1995).
- J. R. Kirtley, M. B. Ketchen, K. G. Stawiasz, J. Z. Sun, W. J. Gallagher, S. H. Blanton, and S. J. Wind, *Appl. Phys. Lett.* 66, 1138 (1995).
- 17. David W. Abraham, C. C. Williams, and H. K. Wickramasinghe, *Appl. Phys. Lett.* **53**, 1503 (1988)
- M. B. Ketchen, D. Pearson, A. W. Kleinsasser, C. K. Hu, M. Smyth, J. Logan, K. Stawiasz, E. Baran, M. Jaso, T. Ross, K. Petrillo, M. Manny, S. Basavaiah, S. Brodsky, S. B. Kaplan, W. J. Gallagher, and M. Bhushan, *Appl. Phys. Lett.* 59, 2609 (1991).
- M. B. Ketchen, D. J. Pearson, K. Stawiasz, C.-K. Hu, A. W. Kleinsasser, T. Brunner, C. Cabral, V. Chandrashekhar, M. Jaso, M. Manny, K. Stein, and M. Bhushan, *IEEE Trans. Appl. Supercond.* 3, 1795 (1993).
- J. Z. Sun, W. J. Gallagher, A. C. Callegari, V. Foglietti, and R. H. Koch, Appl. Phys. Lett. 63, 1561 (1993).
- J. Z. Sun, W. J. Gallagher, and R. H. Koch, *Phys. Rev. B* 50, 13664 (1994).
- See for example the discussion in Ralph A. Sawyer, *Experimental Spectroscopy*, Dover Publications, New York, 1963, p. 34.
- An excellent review of the case for (and against) d-wave superconductivity appears in D. J. Scalapino, *Physics Reports* (Netherlands) 250, 329 (1995).
- 24. For a brief review, see an article by B. G. Levi in *Physics Today*, May 1993, p. 17 and references therein.
- D. A. Wollman, D. J. Van Harlingen, W. C. Lee, D. M. Ginsberg, and A. J. Leggett, *Phys. Rev. Lett.* 71, 2134 (1993)
- P. Chaudhari and Shawn Yu Lin, *Phys. Rev. Lett.* 72, 1084 (1994).
- D. A. Brawner and H. R. Ott, Phys. Rev. B 50, 6530 (1994).
- A. G. Sun, D. A. Gajewski, M. B. Maple, and R. C. Dynes, *Phys. Rev. Lett.* 72, 2267 (1994).
- A. Mathai, Y. Gim, R. C. Black, A. Amar, and F. C. Wellstood, *Phys. Rev. Lett.* 74, 4523 (1995).
- V. B. Geshkenbein, A. I. Larkin, and A. Barone, *Phys. Rev. B* 36, 235 (1987).
- 31. C. C. Tsuei, J. R. Kirtley, C. C. Chi, Lock See Yu-Jahnes, A. Gupta, T. Shaw, J. Z. Sun, and M. B. Ketchen, *Phys. Rev. Lett.* 73, 593 (1994).
- Manfred Sigrist and T. M. Rice, J. Phys. Soc. Jpn. 61, 4283 (1992).
- Bradley J. Roth, Nestor G. Sepulveda, and John P. Wikswo, Jr., J. Appl. Phys. 65, 361 (1988).
- L. N. Bulaevski, V. V. Kuzii, and A. A. Sobyanin, *JETP Lett.* 25, 290 (1977).
- B. I. Spivak and S. Kivelson, *Phys. Rev. B* 43, 3740 (1991).
- J. R. Kirtley, C. C. Tsuei, J. Z. Sun, C. C. Chi, Lock See Yu-Jahnes, A. Gupta, M. Rupp, and M. B. Ketchen, Nature 373, 224 (1995).

Received October 10, 1994; accepted for publication September 13, 1995 John R. Kirtley IBM Research Division, Thomas J. Watson Research Center, P.O. Box 218, Yorktown Heights, New York 10598 (KIRTLEY at YKTVMV, kirtley@watson.ibm.com). Dr. Kirtley is a research staff member in the Physical Sciences Department at the Thomas J. Watson Research Center. He received a B.S. degree in physics from the University of California, Santa Barbara, in 1971, and a Ph.D. degree in physics from the same institution in 1976. He was a postdoctoral fellow and research assistant professor at the University of Pennsylvania from 1976 to 1978. Since 1978 Dr. Kirtley has been at the IBM Thomas J. Watson Research Center, where he has worked in a number of areas, primarily involving transport in solid-state systems. He received IBM Outstanding Innovation Awards in 1981 for work in surfaceenhanced Raman scattering and light emission from tunnel junctions, and in 1986 for work on hot-electron distributions in insulating films of silicon dioxide. Dr. Kirtley is a fellow of the American Physical Society.

Mark B. Ketchen IBM Research Division, Thomas J. Watson Research Center, P.O. Box 218, Yorktown Heights, New York 10598 (KETCHEN at YKTVMV, ketchen@watson.ibm.com). Dr. Ketchen is Director of Physical Sciences at the IBM Thomas J. Watson Research Center. He received a B.S. degree in physics from the Massachusetts Institute of Technology in 1970 and a Ph.D. in physics from the University of California at Berkeley in 1977. He subsequently joined IBM at the Thomas J. Watson Research Center, where he has worked on the physics and technology of semiconductors and superconductors. Dr. Ketchen is a fellow of the American Physical Society, a senior member of the Institute of Electrical and Electronics Engineers, and a member of the IBM Academy of Technology.

Chang C. Tsuei IBM Research Division, Thomas J. Watson Research Center, P.O. Box 218, Yorktown Heights, New York 10598 (TSUEI at YKTVMV, tsuei@watson.ibm.com). Dr. Tsuei is a research staff member in the Physical Sciences Department at the Thomas J. Watson Research Center. He received a B.S. degree in mechanical engineering from the National Taiwan University in 1960, and M.S. and Ph.D. degrees in materials science from the California Institute of Technology in 1963 and 1966, respectively. He subsequently joined IBM at the Thomas J. Watson Research Center, where he has worked in the field of superconductivity. In 1990 he received an IBM Outstanding Technical Achievement Award for his work on grain-boundary junctions and devices in cuprates. Currently his research interests are pairing symmetry and mechanisms in high-temperature superconductors. Dr. Tsuei is a fellow of the American Physical Society.

Jonathan Z. Sun IBM Research Division, Thomas J. Watson Research Center, P.O. Box 218, Yorktown Heights, New York 10598 (JONSUN at YKTVMV, jonsun@watson.ibm.com). Dr. Sun is a research staff member in the Physical Sciences Department at the Thomas J. Watson Research Center. He received his B.S. degree in physics from Fudan University, Shanghai, China, in 1984, and M.S. and Ph.D. degrees in applied physics from Stanford University in 1986 and 1989, respectively. He worked at Superconductor Technologies Inc. in Santa Barbara, California, from 1989 to 1992, subsequently joining IBM at the Thomas J. Watson Research Center, where he has worked on oxide thin-film device physics in areas of high- $T_{\rm c}$ SQUID magnetometers, and in magnetoresistive conducting oxide thin films. Dr. Sun is a member of the American Physical Society and the Materials Research Society.

William J. Gallagher IBM Research Division, Thomas J. Watson Research Center, P.O. Box 218, Yorktown Heights, New York 10598 (GLGR at YKTVMV). Dr. Gallagher is a

research staff member at the IBM Thomas J. Watson Research Center. He joined IBM in 1978 after receiving his B.S. in physics summa cum laude from Creighton University in 1974 and his Ph.D. in physics from MIT. He is the manager of the Exploratory Cryogenics research group and an associate director of the AT&T-IBM-MIT-founded Consortium for Superconducting Electronics. Dr. Gallagher's research activities are primarily in the physics and applications of superconducting electronic devices. In 1989, he received an IBM Outstanding Technical Achievement Award for elucidating the anisotropic nature of high-temperature superconductivity in YBa₂Cu₂O₇. Dr. Gallagher is a fellow of the American Physical Society and a member of the IEEE. He has served as assistant to the chairman of the APS Panel on Public Affairs and on the Executive Committee of the APS Forum on Physics and Society. He has also served on study panels convened by the National Research Council, the National Science Foundation, the Office of Naval Research, and the Office of Technology Assessment.

Lock See Yu-Jahnes Cooper & Dunham LLP, 1185 Avenue of the Americas, New York, New York 10036.

Arunava Gupta IBM Research Division, Thomas J. Watson Research Center, P.O. Box 218, Yorktown Heights, New York 10598 (AGUPTA at YKTVMV, agupta@watson.ibm.com). Dr. Gupta is a research staff member in the Physical Sciences Department at the Thomas J. Watson Research Center. He received an M.S. degree in chemistry from the Indian Institute of Technology in 1976, and a Ph.D. degree in chemical physics from Stanford University in 1980. He subsequently joined Allied Signals in Morristown, New Jersey, where he worked on catalysis and laser processing of materials. In 1985 Dr. Gupta joined the Thomas J. Watson Research Center, where he has worked on various photothermal and photochemical laser techniques for processing and patterning of materials. He is currently involved in studying the growth and properties of superconducting and magnetic oxide materials. Dr. Gupta is a member of the Materials Research Society and the American Physical Society.

Kevin G. Stawiasz IBM Research Division, Thomas J. Watson Research Center, P.O. Box 218, Yorktown Heights, New York 10598 (STAWASZ at YKTVMV, stawasz@watson.ibm.com). Mr. Stawiasz is a senior associate engineer in the High-Speed Test and Measurement group at the Thomas J. Watson Research Center. He received a B.S. degree in electrical engineering and physics from Lawrence Institute of Technology in 1987, and an M.S. degree in physics from the University of Illinois in 1989. He subsequently joined IBM at the Thomas J. Watson Research Center, where he worked on processing technology for low-T_c superconducting devices until 1994. He is currently working on automated testing of VLSI circuits and optoelectronic devices and circuits. Mr. Stawiasz is a member of the Institute of Electrical and Electronics Engineers.

Shalom J. Wind IBM Research Division, Thomas J. Watson Research Center, P.O. Box 218, Yorktown Heights, New York 10598 (WIND at WATSON). Dr. Wind is a research staff member in the Silicon Technology Department at the Thomas J. Watson Research Center. In 1987 he received a Ph.D. degree in physics from Yale University, where he studied electron quantum transport in nanostructures. He began his work at the Research Center in the Electron Beam Technology area in 1987. Since that time, Dr. Wind has been involved in high-resolution electron-beam lithography and processes, the fabrication of nanostructures and exploratory devices, and the study of ultrasmall devices at the limits of fabrication feasibility.